How Viral Interactions in Coinfection Shape Viral Kinetics

A Thesis

Presented in Partial Fulfillment of the Requirements for the

Degree of Master of Science

with a

Major in Bioinformatics and Computational Biology

in the

College of Graduate Studies

University of Idaho

by

Joseph DeAguero

Major Professor: Christopher H. Remien, Ph.D.

Committee Members: James Foster, Ph.D.; Tanya Miura, Ph.D.;

Amber M. Smith Ph.D.

Department Administrator: David Tank, Ph.D.

December 2018

Authorization to Submit Thesis

This thesis of Joseph DeAguero, submitted for the degree of Master of Science with a major in Bioinformatics and Computational Biology and titled "How Viral Interactions in Coinfection Shape Viral Kinetics," has been reviewed in final form. Permission, as indicated by the signatures and dates given below, is now granted to submit final copies to the College of Graduate Studies for approval.

Major Professor: _____Date_____
Christopher H. Remien, Ph.D.

Committee Members: _____Date_____
James Foster, Ph.D.

_____Date_____
Tanya Miura, Ph.D.

_____Date_____
Amber M. Smith, Ph.D.

Department Administrator: _____Date_____
David Tank, Ph.D.

Abstract

Coinfections with more than one respiratory virus can enhance or inhibit virus growth kinetics and disease severity depending on the underlying mechanism of interaction. Although some mechanisms are known (e.g., enhanced virus entry), viral-viral coinfections are only beginning to be examined in the laboratory and clinic. Thus, to understand how different mechanisms of viral interactions can affect viral titer kinetics, we developed and analyzed a mathematical model. Here, we focused on how coinfection leading to increases or decreases in viral infection rate, viral production rate, viral clearance rate, and infected cell death rate alters viral kinetics. While each of these types of interactions can lead to increases or decreases in total virus produced, each interaction type alters the viral kinetics in characteristic ways. We found that decreasing the viral clearance rate leads to the largest increase in total virus produced relative to coinfection without direct interactions. We varied the strength of interactions and timing of viral infections to determine how these critical factors impact results. Our results suggest that the mechanisms underlying virus-virus interactions and the relative timing of infection of the two viruses impact the rate of viral titer increase, the timing of peak, and the rate of viral titer decrease after peak, and thus the total duration and severity of disease.

Acknowledgements

During the journey to complete work on my thesis, there are several individuals who have helped me along the way. First, I would like to thank Amber Smith. I am grateful she gave me the opportunity to work in her lab and took the time to help with my research. I would also like to thank Chris Remien for being a supportive advisor and taking the time to assist and guide me through my research project. Chris always portrayed a positive attitude and this helped the research move along. Amber and Chris were a great team. I fully enjoyed every meeting we had together and always walked away with a better sense of the topic at hand. Additionally, I would like to thank the rest of my committee, Tanya Miura and James Foster. Tanya Miura allowed me to work in her lab and learn some basic laboratory techniques, which were crucial to my understanding of the biology behind my research. James Foster was always helpful with questions I had and always gave useful comments for my thesis.

Last but not least, I would like to thank my wife Ashley DeAguero. She was supportive and was crucial to my success. I owe all my success to her and the commitment she made to taking care of our boys while I worked on my Masters. I would also like to thank my wonderful boys, Elijah and Dylan. After long days of working on my research, the boys were always excited to see me and this helped me stay on track to finish.

Table of Contents

List of Tables

List of Figures

CHAPTER 1

Introduction

During a respiratory infection, a host can be infected by one or more viruses. These respiratory viruses target the same cells, epithelial cells in a host, and can cause a range of symptoms including death among young children, the elderly, and immunocompromised individuals [1, 2]. Our understanding of how virus-virus interactions in coinfection impact disease severity is limited. Knowing how viruses interact within the host is important in determining whether specific virus-virus combinations increase or decrease disease severity. In this chapter we will introduce general information about respiratory viruses and respiratory coinfections, including the history of mathematical modeling the spread of virus within a host.

1.1 Respiratory Virus Infection and Coinfection

Respiratory viruses such as influenza virus (IV), respiratory syncytial virus (RSV), rhinovirus (RV), parainfluenza virus (PIV), human metapnuemovirus (hMPV), adenoviruses (ADV), and coronavirus (CoV) share many common features, and infection by each leads to similar symptoms for the host (Table 1.1). Infection occurs when a person breaths virus through the nose or mouth, leading to viral infection of epithelial cells in the respiratory tract. As the virus spreads and infects epithelial cells, more virus is produced. After a person is infected by one of the viruses, the person will become infectious for four to seven days until the innate and adaptive immune systems clear the virus from the host. The innate response is the basic response to general pathogens, and works towards removal of foreign material while initiating a more specific response, the adaptive response. Adaptive responses typically take around seven to ten days to develop the specific immune cells to target the pathogen, but once the cells are developed, the host develops immunological memory for the pathogen and the removal time

is reduced if the pathogen is encountered again.

Many respiratory viruses target similar cells and circulate in the population at the same time, so it is possible that an individual may be coinfected with multiple viruses at the same time. Indeed, studies have shown that IV, RV, RSV, PIV, hMPV, ADV, and CoV can simultaneously infect humans [3–9]. The few controlled studies of respiratory coinfection have shown a variety of effects on viral kinetics. For example, PIV has been shown to increase the viral load of IV, *in-vitro* [10], while RV reduces viral load of IV within a mouse, *in-vivo* [11]. While there are relatively few empirical studies that track viral kinetics in coinfection with respiratory viruses, we can imagine that coinfection could alter viral dynamics in numerous ways, with some combinations increasing the severity of infection while others reduce disease severity.

1.2 Comparison of Respiratory Viruses

Respiratory viruses vary in their seasonality, number of serotypes, and availability of a vaccine (Table 1.1). In the United States, seasonality of the viruses vary, but all peak during the winter. RV is detected year round but is less prevalent in the summer months [12]. The respiratory viruses discussed here all have multiple types and some are specifically known for the differences in types. For example, IV, is known by the different subtypes [13]. Influenza viruses are further subdivided into different subtypes based on the surface glycoproteins, haemagglutinin (HA) and neuraminidase (NA) [14]. The recombination of these proteins is the cause of the major IV outbreaks throughout the years [15]. The two subgroups of RSV are divided into two antigenic subgroups A and B [16]. Most of the viruses do not have a vaccine or treatment, though there are vaccines and therapeutics available for IV and a prophylactic for RSV. Every year a vaccine is developed to target all four of the serotypes of IV [17]. For high risk infants there is an antibody prophylactic, Palivizumab, which targets the fusion protein of RSV

inhibiting its entry into the cell and thereby preventing infection [18].

Table 1.1: Comparisons of respiratory viruses. Comparison of different respiratory viruses, including influenza virus (IV), respiratory syncytial virus, (RSV), rhinovirus (RV), parainfluenza (PIV), human metapneumovirus (hMPV), adenovirus (ADV), and coronaviruses (CoV).

Virus	Baltimore Classification	Seasonality	Vaccine	Type
IV	(-)ssRNA	October-May [19]	Quadrivalent vaccine [17]	A, B, C, D [13]
RSV	(-)ssRNA	September-May [12]	N/A	1 with antigenic groups A, B [12]
RV	(+)ssRNA	August-April [20]	N/A	160 with 3 species (A, B, and C) [21]
PIV	(-)ssRNA	Varies depending on serotype [22]	N/A	5 with 2 genera: 4a and 4b [8]
hMPV	(-)ssRNA	November-February [23]	N/A	2 [24]
ADV	dsDNA	November-May [25]	N/A	51 [25]
CoV	(+)ssRNA	November-May [26]	N/A	4 [27]

1.3 Viral Load Kinetics

Most viruses increase exponentially for 3-4 days and for acute infections like respiratory viruses, the virus is usually cleared within 10 days [28]. Several techniques have been developed to quantify the amount of virus in a given volume, also known as viral load or viral titers, including plaque assays, endpoint dilution, and quantitative polymerase chain reaction (qPCR)[29–31]. Each type of quantification provides information on the viral load, but they measure fundamentally different quantities. Plaque assays calculate the virus concentration in terms of the infectious dose by determining the number of plaque forming units (PFU). Endpoint dilution is a measure of infectious virus titers and quantifies the amount of virus required to kill half of the infected cells or to produce a cytopathic effect in half of inoculated tissue culture cells ($TCID_{50}$). Another laboratory

technique, qPCR, utilizes polymerase chain reaction chemistry to amplify viral DNA or RNA to produce high enough concentrations for detection and quantification by fluorescence.

1.4 Within-Host Modeling

Mathematical modeling has been used for over twenty years to better interpret viral kinetic data and to predict effects of treatment [32–38]. In an effort to understand human immunodeficiency virus (HIV) infection, mathematical models ('viral dynamics models') were developed to predict viral titers of HIV in infected patients [39, 40]. The viral dynamics model uses a system of three coupled differential equations to track the number of target cells, infected cells, and free virus in the host over time and is parameterized with measurements of viral titers over time. The model includes replenishment of cells, cell death, viral infection of target cells, virus production by infected target cells, and clearance of the virus by immune responses. When parameterized with viral titer data from HIV positive patients, the model successfully predicted the virus peak and matched overall viral kinetics [39, 40]. Because of the success in HIV, numerous models have since been developed to study other viruses, including Hepatitis B and C viruses, West Nile virus, Dengue virus, yellow fever virus, Zika virus, BK virus, Human Papilloma virus, ADV, and IV, often with modifications to capture details specific to a particular virus [34–36, 41–50]. The time scale and dynamics of these viruses may differ, but the foundation of the viral dynamics model can help predict the viral kinetics of each of these viruses within a host.

Viral dynamics models have been developed for respiratory viruses including IV. To account for the difference in infectious period of IV compared to HIV, a simplified viral dynamics model called the target cell-limited model (TCL) was developed that excludes the replenishment of target cells, as target cells are not generated in significant quantity

over the time period of IV infection [51]. The model consists of four classes: target cells (T), infected cells in the eclipse phase (E), infected cells secreting virus (I), and free virus (V). The model is given by Equations (1.1)–(1.4). Target cells are infected by the virus at per capita rate βV. The model excludes cell regeneration due to the short time scale of IV infection. Once infected, cells enter the eclipse phase, at which point the cells are infected but not yet producing virus. Cells transition from the eclipse phase to an active infection phase at per capita rate k. Infected cells are removed at per capita rate δ. This removal may be due to apoptosis or removal by immune cells. Free virus is produced at rate p virus per cell per day, and is cleared at per capita rate c per day. This model also includes a new state variable to capture the eclipse phase of IV infection, the time it takes a virus to enter a cell and start producing virus. The inclusion of an eclipse was shown by Baccam et al. to not be statistically significant but was still included because it is biologically relevant to include a period before IV can start producing more virus [51]. In a well-mixed homogeneous environment, these assumptions lead to the following system of ordinary differential equations:

$$\frac{dT}{dt} = -\beta TV \tag{1.1}$$
$$\frac{dE}{dt} = \beta_1 TV_1 - k_1 E_1 \tag{1.2}$$
$$\frac{dI}{dt} = k_1 E_1 - \delta_1 I_1 \tag{1.3}$$
$$\frac{dV}{dt} = p_1 I_1 - c_1 V_1. \tag{1.4}$$

Although there is a well-established history of modeling within host dynamics of infection of a single virus, modeling coinfection is still in its infancy [35]. Recently, a coinfection model was developed to study two respiratory viruses that simultaneously infect a host [52]. The model uses the foundation of the target cell-limited model,

but includes three additional classes to capture the dynamics of a second virus that simultaneously infects target cells. Direct interactions were not included in the model; instead, the only interaction between the viruses is via indirect competition for target cells. In analyzing this model, Pinky and Dobrovolny [52] found that the virus with the largest growth rate outcompetes the virus with a lower growth rate. In Chapter 2, we will extend this work to include direct interactions between viruses, where one virus affects the growth and survival of the other virus during coinfection.

CHAPTER 2

Modeling the Kinetics of Viral-Viral Coinfection

2.1 Introduction

During a respiratory infection, there is a possibility that multiple viruses are present and working in conjunction to cause disease [3, 4, 6]. Several respiratory viruses, including rhinovirus (RV), respiratory syncytial virus (RSV), influenza A and B viruses (IAV, IBV), human metapneumovirus (hMPV), human parainfluenza viruses (PIV), adenoviruses (ADV), and coronavirus (CoV), have been found concurrently within a host [3, 4, 6, 9, 13, 53–57]. Although ADV is the most common virus found in multi-virus infections [54], several other virus pairings have been detected (e.g., RV and RSV, and RSV and IV) [3, 4, 6, 54, 55]. Children are more likely to be infected with multiple respiratory viruses, and studies have shown that up to 30 percent of infected children are infected with more than one respiratory virus [9, 57].

Several mechanisms have been shown by which viruses interact during coinfection [10, 11, 58]. These mechanisms can be either beneficial or detrimental to the growth of each virus. One way that viruses interact is through competition for target cells. Mathematical modeling has shown that in this type of interaction, the virus with the larger infection rate or the larger production rate would likely out compete the other virus [52]. However, this is not the only form of interaction. Studies have indicated that viruses can also interact through other mechanisms like when one virus reduces the infectivity of another virus by blocking the entry to a cell or reducing susceptibility [7, 11, 58–61]. Another example is enhanced cell-cell fusion, which results in increased viral entry into cells [10]. Goto et al. [10] showed that the rate IAV infects target cells was enhanced due to the presence of PIV. Other mechanisms have been proposed for virus-virus interactions (e.g., altered host susceptibility due to altered receptor expression,

modification of the interferon-induced antiviral state, or viral exclusion), but have not been shown in cell culture or an animal model for respiratory viruses [62]. Classifying the mechanisms involved in respiratory coinfections and their effects on viral dynamics will aid our understanding about why some respiratory virus pairs are more frequently observed than others [6, 7, 54, 55].

Mathematical modeling has been used to study the dynamics of single infections, including HIV, hepatitis B, hepatitis C viruses (HCV, HBV), and IAV [34–36, 39–42], and to predict the time course of viral loads within a host. With the success of these single infection models, Pinky and Dobrovolny [52] developed a respiratory viral-viral coinfection model that focused on target cell competition as the mechanism of interaction between viruses.

Here, we build on this work by using mathematical modeling to test how different mechanisms of interaction alter viral load dynamics. We expand the target cell-limited model [51] to include states for two viruses and assess direct and indirect modes of interactions between the viruses. We examine numerous scenarios in which one virus enhances or inhibits different aspects of the infection (e.g., virus infectivity, production, clearance, and infected cell clearance). In addition, we assess how viral load dynamics change given different timings between infections. The results show the range of possible viral load dynamics given a variety of interaction mechanisms, including those outside the range previously studied experimentally.

2.2 Methods

2.2.1 Coinfection Model Without Direct Interactions

To study how various types of virus-virus interactions affect viral kinetics, we extend the coinfection model developed by Pinky and Dobrovolny [52]. In their model, the only

interaction between viruses is through competition for target cells. We will refer to this model as the baseline model with states shown in Figure 2.1. In this model target cells (T) are infected by both viruses (V_1) and (V_2) at per capita rates $\beta_1 V_1$ and $\beta_1 V_2$ per day, respectively, and cells can only be infected by one of the viruses. We excluded the possibility for coinfection within cells for simplicity. The remaining populations follow the same structure as the TCL model, yielding the baseline model presented in Pinky and Dobrovolny [52]:

$$\frac{dT}{dt} = -\beta_1 T V_1 - \beta_2 T V_2 \tag{2.1}$$
$$\frac{dE_1}{dt} = \beta_1 T V_1 - k_1 E_1 \tag{2.2}$$
$$\frac{dI_1}{dt} = k_1 E_1 - \delta_1 I_1 \tag{2.3}$$
$$\frac{dV_1}{dt} = p_1 I_1 - c_1 V_1 \tag{2.4}$$
$$\frac{dE_2}{dt} = \beta_2 T V_2 - k_2 E_2 \tag{2.5}$$
$$\frac{dI_2}{dt} = k_2 E_2 - \delta_2 I_2 \tag{2.6}$$
$$\frac{dV_2}{dt} = p_2 I_2 - c_2 V_2 \tag{2.7}$$

2.2.2 Coinfection Model with Direct Interactions

To study the effects of virus-virus interactions, the parameters for both viruses were set equal, so that the only variation in the model is due to virus-virus interactions (Table 2.1). Because Virus 1 and Virus 2 are identical, modifying the transition rates for Virus 1 will be the same as for Virus 2. We focused on the presence of Virus 2 modifying the infection rate β_1, virus production rate p_1, infected cell death rate δ_1, and the viral clearance rate c_1 of Virus 1. Two functions, Equation (2.8) and Equation (2.9), were used to modify the rates to represent an increase or decrease to the specific parameter,

respectively:

$$\alpha(V_2) = 1 + \kappa V_2 \tag{2.8}$$

$$\zeta(V_2) = \frac{1}{1 + \kappa V_2}. \tag{2.9}$$

Equation (2.8) is an increasing function while Equation (2.9) is a decreasing function of Virus 2 (V_2). We modify the rates by multiplying Equation (2.8) or (2.9) by the rate affected by Virus 2. For example if the infection rate (β_1) of Virus 1 is increased by Virus 2, the new infection rate becomes $(1 + \kappa V_2)\beta_1 T V_1$. The parameter κ represents the strength of the interaction. If $\kappa = 0$, then the baseline model is achieved.

Equation (2.8) and Equation (2.9) were individually multiplied by each rate of the baseline model, the model without direct interactions ($\kappa = 0$), for a total of eight models. The total virus produced or area under the curve (AUC) was calculated using MATLAB's

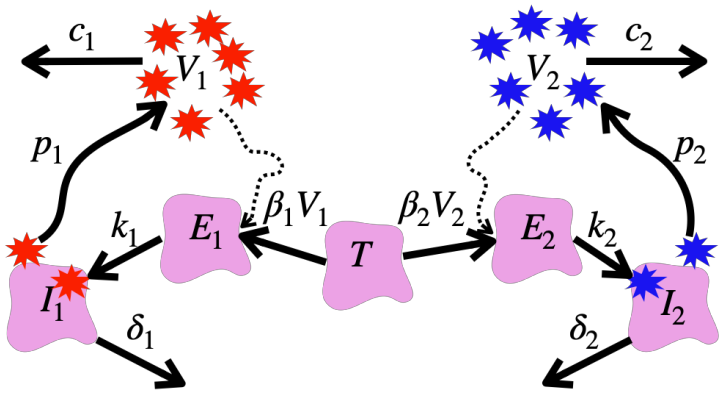

Figure 2.1: Coinfection model schematic. Schematic diagram of the mathematical model presented in Pinky and Dobrovolny [52] for viral coinfections. Target cells (T) are concurrently infected by Virus 1 (red; V_1) and Virus 2 (blue; V_2). Once infected, cells undergo an eclipse phase (E_1 and E_2) before actively producing virus (I_1 and I_2). Each parameter is labeled with subscripts 1 and 2 to denote Virus 1 (V_1) and Virus 2 (V_2), respectively.

Table 2.1: Coinfection model parameter descriptions. All parameters used in Equations (2.1)–(2.7) were taken from Smith et al. [63]. The parameters were calibrated using viral load data from mice infected with influenza virus A/Puerto Rico/8/34 (PR8). Here, $i = 1, 2$ denotes Virus 1 and Virus 2, respectively.

Parameter	**Description**	**Units**	**Value**
β_i	Virus infectivity	$(\text{TCID}_{50})^{-1}\text{day}^{-1}$	2.8 x 10^{-6}
k_i	Eclipse phase	day^{-1}	4.0
δ_i	Infected cell death	day^{-1}	0.89
p_i	Virus production	$(\text{TCID}_{50})^{-1}\text{day}^{-1}$	25.1
c_i	Virus clearance	day^{-1}	28.4
T_0	Initial uninfected cells	cells	10^7
$E_i(0)$	Initial eclipse cells	cells	0
$I_i(0)$	Initial infected cells	cells	0
$V_i(0)$	Initial virus	TCID_{50}	2
κ	Strength of interaction	$(\text{TCID}_{50})^{-1}$	See text

trapz function for the baseline and the eight models with different interactions. We compared the total virus produced (V_{int}) of both viruses for each of the eight models with an interaction to the AUC of the virus of the baseline (V_{base}) (e.g., $\kappa = 0$). The fold change (V_{fold}) in virus produced in coinfection due to virus-virus interaction relative to baseline was calculated as:

$$V_{fold} = \frac{V_{int} - V_{base}}{V_{base}}. \tag{2.10}$$

The system of differential equations (Equations (2.1)–(2.9)) was numerically solved with the MATLAB (R017b) ODE solver *ode15s*. We use the parameters from Smith et al. [63], which were calibrated using viral load data from mice infected with IAV. Balb/cJ mice were infected with a mouse adapted IAV. The lungs were harvested and the infectious viral load (TCID_{50}) was measured.

2.3 Results

We developed a mathematical model of virus-virus coinfection that allows for viral enhancement or inhibition of one virus due to the presence of another virus (Equations (2.1)–(2.7) with Equations (2.8) or (2.9)). Viral kinetics in coinfection depend on the underlying mechanism of interaction, the interaction strength, and the relative timing of infection of the two viruses. Typically, in a single infection, viral infection kinetics are characterized by two phases, with an initial exponential increase in viral titers, a peak, and a later a exponential decay in viral titers [51, 64]. To study how coinfection alters these typical viral kinetics, we modify positively or negatively the virus infection rate, rate of virus production, virus clearance rate, and infected cell death rate to determine how various mechanisms of interactions during coinfection alter viral kinetics. Further we tested how these effects on viral kinetics depend on the strength of interaction and relative timing of the infection of the two viruses.

2.3.1 Simultaneous Coinfection

We first studied the case where two viruses are introduced at the same time. We assume that the two viruses share identical parameters. Because in all cases Virus 2 is only indirectly affected by Virus 1, the only interaction affecting Virus 2 is from competition for target cells. Thus, the viral growth curves for Virus 2 maintain similar shape to the baseline case where there are no interactions (Figures 2.2–2.3). In all cases, Virus 2 maintains nearly identical rates of increase and decay as when there is no interaction. In cases where there is viral enhancement, Virus 2 peaks at lower values than baseline, while when there is viral inhibition, Virus 2 peaks at higher values than baseline.

Enhanced Infection

We studied viral enhancement of Virus 1 from the presence of Virus 2 due to increased infection rate (β_1+), increased viral production (p_1+), decreased viral clearance (c_1-), and decreased infected cell death rate (δ_1-) (Figure 2.2). Depending on the mechanism, Virus 1 titers will increase during the growth phase or the decay phase, or both (Figure 2.2). When the infection rate of virus 1 is increased (β_1+) by Virus 2, Virus 1 titers peak earlier compared to the baseline and decrease at the same rate as the baseline (Figure 2.2A). When the viral production is increased (p_1+) or viral clearance rate is decreased (c_1-) by Virus 2, the peak of Virus 1 is increased during the growth phase and decays at a faster rate during the decay phase (Figure 2.2B–C). The rate at which Virus 1 decays during the decay phase varies for the two interactions, p_1+ and c_1-, and this is shown with different strengths of interactions (κ). When infected cell death rate is decreased (δ_1-) by Virus 2, there is no change in the rate during the growth phase compared to the baseline and there is no decay in Virus 1 titers (Figure 2.2D). The smallest fold change in virus is when the infection rate is increased (β_1+) and the largest fold change is when the viral clearance rate is decreased (c_1-) (Figure 2.2E).

Inhibited Infection

We studied viral inhibition of Virus 1 from the presence of Virus 2 due to decreased infection rate (β_1-), decreased viral production (p_1-), increased viral clearance (c_1+), and increased infected cell death rate (δ_1-). When Virus 1 is inhibited, the titers will be lower than the baseline and Virus 1 may be eliminated from the host depending on the strength of interaction (Figure 2.3). Initially during the growth phase, between zero and one day post infection, there is no difference in the rate of viral increase for β_1-, p_1-, c_1+, and δ_1- compared to the baseline. When the infection rate is decreased (β_1-), the

peak of Virus 1 is lower, but the virus decays starting at a lower titer at the same rate as the baseline (Figure 2.3A). Decreasing the viral production rate (p_1-) and increasing the viral clearance rate (c_1+) have similar dynamics; Virus 1 titers peak at a lower value and decay at a faster rate compared to the baseline (Figure 2.3B–C). The virus obtains the highest viral titer peak when the infected cell death rate is increased (δ_1-), but Virus 1 decays at a faster rate while approaching zero or removal from the host (Figure 2.3D). Each case produces the same fold change in total virus produced, even though the viral dynamics for each scenario produce fundamentally different shapes. This is because each modified rate is decreasing different parts of the viral curve, growth or decay phase of Virus 1. (Figure 2.3E).

Strength of Interaction

We varied the strength of interaction (κ) to determine its effect on viral titer dynamics. In Figure 2.4, Virus 1 titers increase as the strength of the interaction (κ) increases. Even for a small change, κ =1e-6 to 1e-4 per virus, increasing the viral production rate (p_1) increases the viral titers of Virus 1 by a log (Figure 2.4B). The timing of the peak occurs earlier for all cases except when the infected cell death rate is reduced (δ_1-) (Figure 2.4).

Larger strengths of interactions (κ) further decrease the titers of Virus 1 (Figure 2.5). Virus 1 may even be removed from the host within two days post-infection if κ is larger than 1e-6 per virus. Decreasing the viral production rate (p_1-) or increasing the viral clearance rate (c_1+) produce similar curves given similar strength of interactions (Figure 2.5B–C).

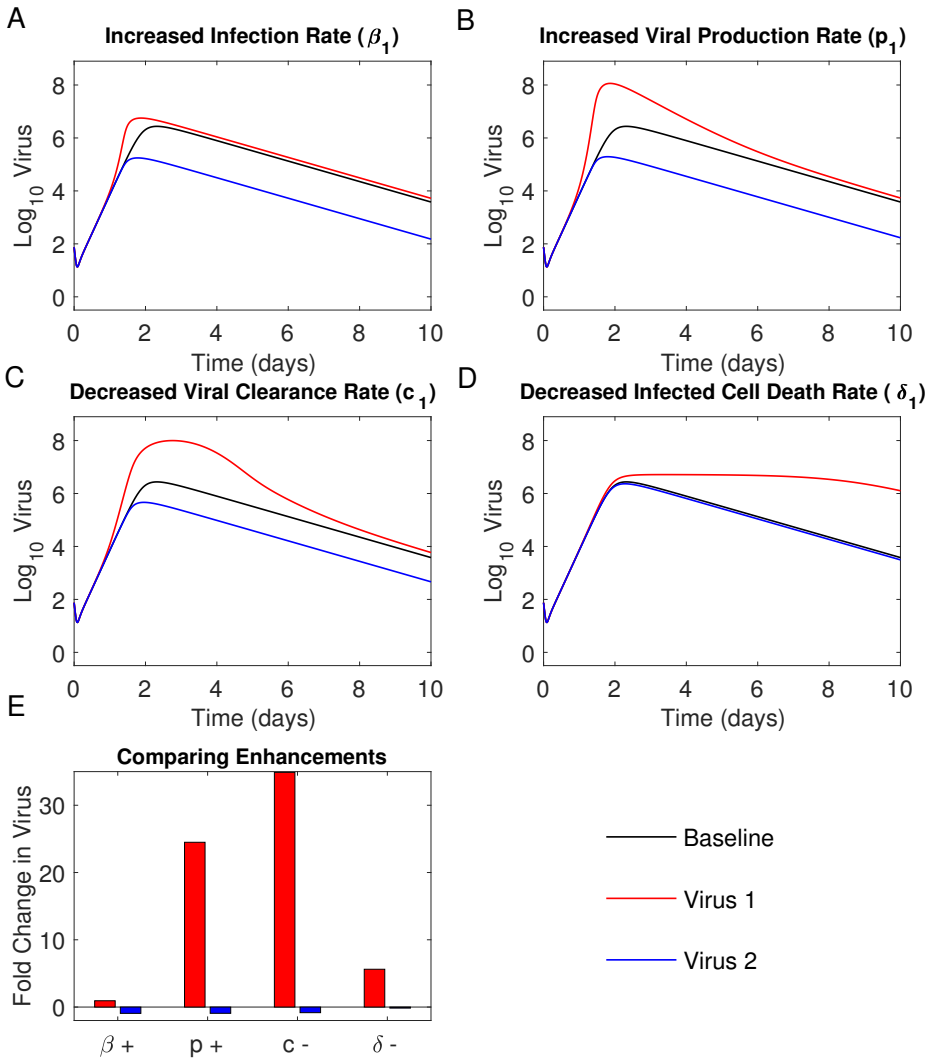

Figure 2.2: Viral kinetics during positive virus interference. Equations (2.1)-(2.7) together with Equation (2.8) or Equation (2.9) were used to simulate the interaction of two viruses in cases where the interaction of Virus 2 on Virus 1 leads to an increase in viral titers. Virus 1 (red), Virus 2 (blue), and virus without interactions (black line; "baseline"). Changes in viral load are shown for (A) increasing the rate of infection (β_1+) with Equation (2.8), (B) increasing the rate of viral production (p_1+) with Equation (2.8), (C) decreasing the rate of infected cell death (δ_1-) with Equation (2.9), or (D) decreasing the rate of viral clearance (c_1-) with Equation (2.9). (E) The relative change in viral loads compared to the baseline for Virus 1 (red bars) and Virus 2 (blue bars) for the indicated interaction. The strength of interaction was set to $\kappa = 1e-4$ per virus. All other parameters are given in Table 2.1.

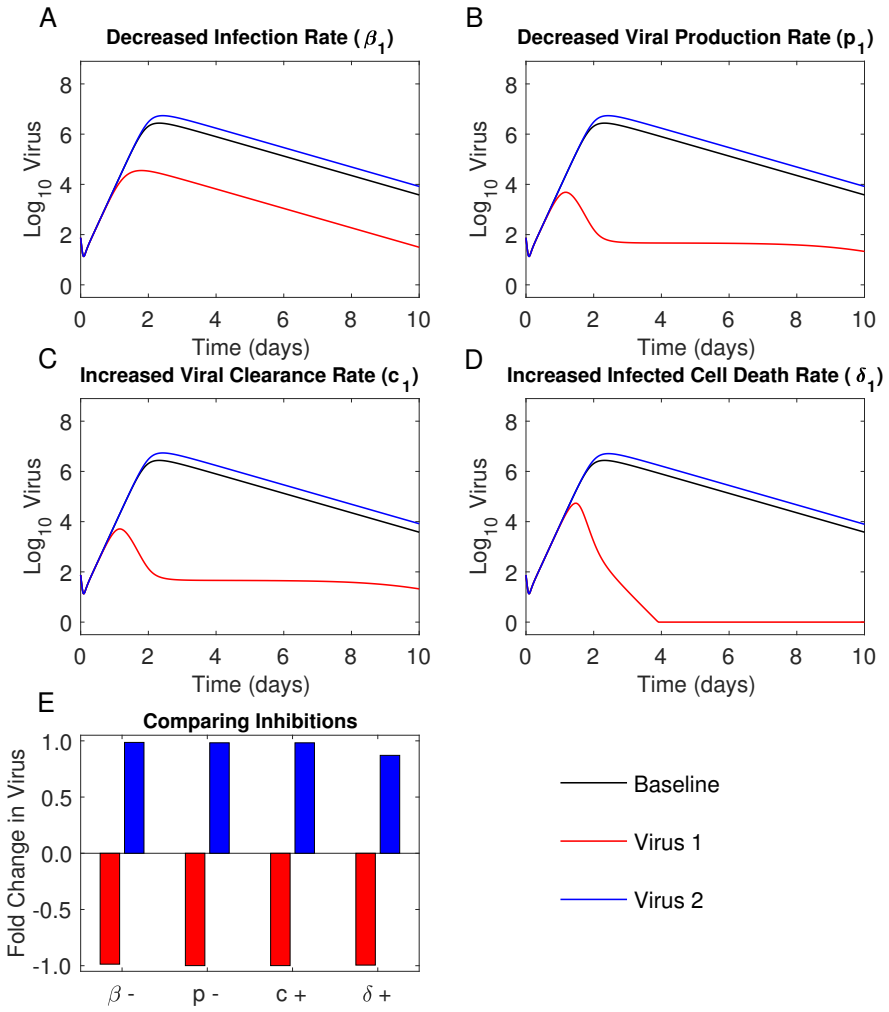

Figure 2.3: Viral kinetics during negative virus interference. Equations (2.1)–(2.7) together with Equation (2.8) or Equation (2.9) were used to simulate the interaction of two viruses in cases where the effect of Virus 2 on Virus 1 leads to an decrease in viral titers. Virus 1 (red), Virus 2 (blue), and virus without interactions (black line; "baseline"). Changes in viral loads are shown for (A) decreasing the rate of infection (β_1-) with Equation (2.9), (B) decreasing the rate of viral production (p_1-) with Equation (2.9), (C) increasing the rate of infected cell death (δ_1+) with Equation (2.8), or (D) increasing the rate of viral clearance (c_1+) with Equation (2.8). (E) The relative change in viral loads compared to the baseline for Virus 1 (red bars) and Virus 2 (blue bars) for the indicated interaction. The strength of interaction was set to κ=1e-4 per virus. All other parameters are given in Table 2.1.

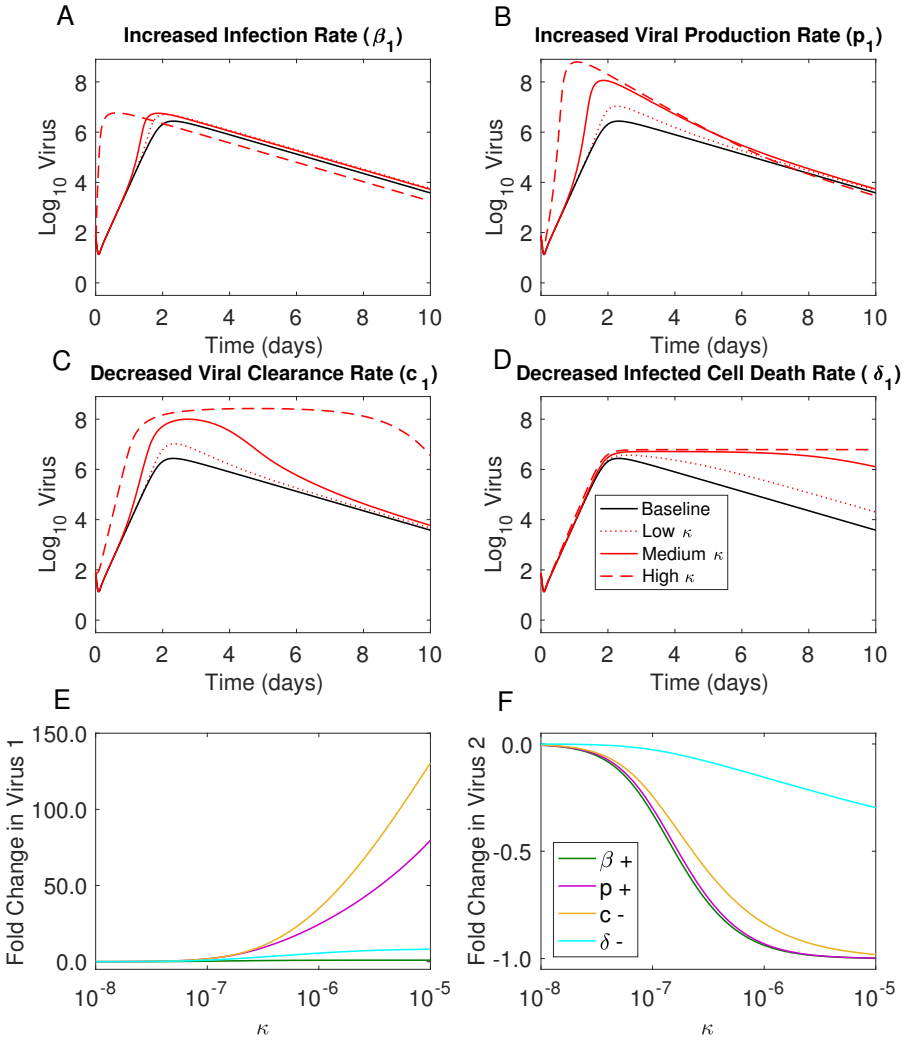

Figure 2.4: Effective interaction strength during positive virus interference. Equations (2.1)–(2.7) together with Equation (2.8) or Equation (2.9) were used to simulate the interaction of two viruses with varying interaction strengths (κ). Virus 1 with varying interaction strengths (κ) (red) and virus without interactions (black line; "baseline"). Changes in viral loads are shown for (A) increasing the rate of infection (β_1+) with Equation (2.8) for κ =1e-5, 1e-3, or 10 per virus, (B) increasing the rate of viral production (p_1+) with Equation (2.8) for κ =1e-6, 1e-4, or 0.1 per virus, (C) decreasing the rate of infected cell death (δ_1-) with Function (2.9) for κ = 1e-6, 1e-5 or 1 per virus, or (D) decreasing the rate of viral clearance (c_1-) with Function (2.9) for κ =1e-6, 1e-4, or 1 per virus. The strength of interaction compared to viral loads for (E) Virus 1 or (F) Virus 2 for the given interactions. Parameters are given in Table 2.1.

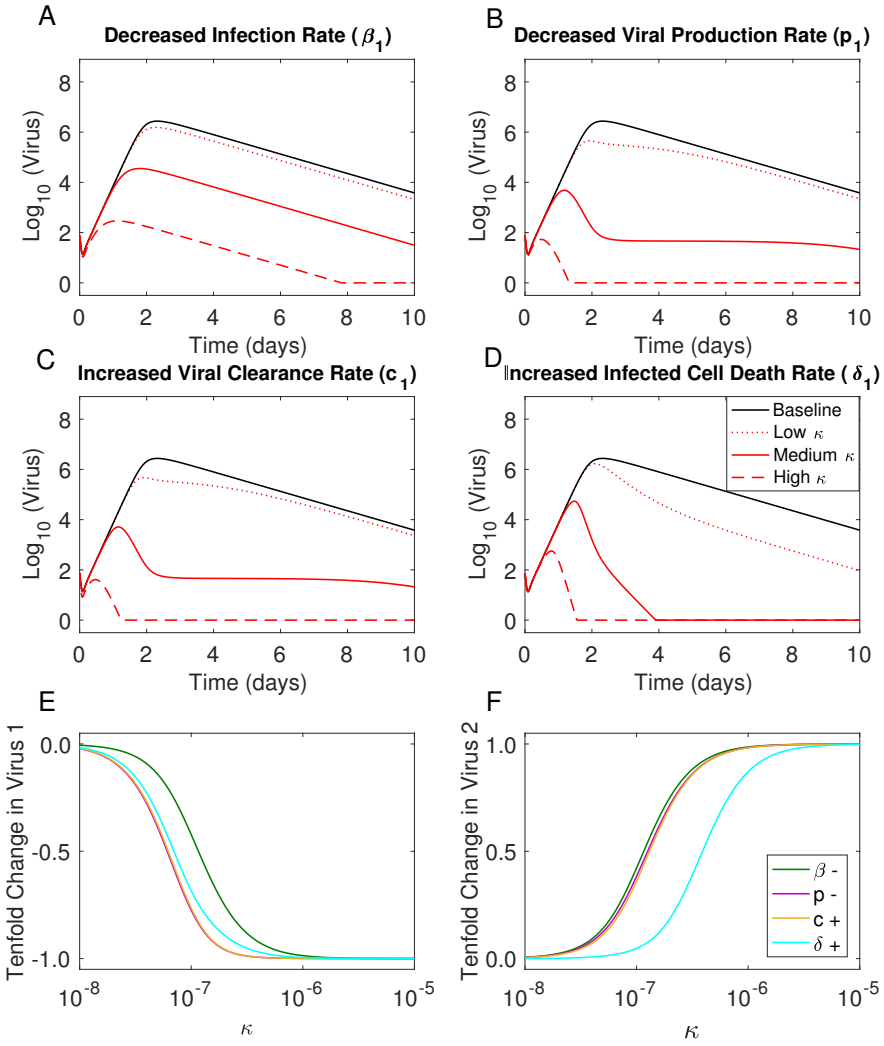

Figure 2.5: Effective interaction strength during negative virus interference. Equations (2.1)–(2.7) together with Equation (2.8) or Equation (2.9) were used to simulate the interaction of two viruses with varying interaction strengths (κ). Virus 1 with varying interaction strengths (κ) (red) and virus without interactions (black line; "base"). Changes in viral loads are shown for (A) decreasing the rate of infection (β_1-) with Equation (2.9) for κ =1e-5, 1e-3, or 10 per virus, (B) decreasing the rate of viral production (p_1-) with Equation (2.9) for κ =1e-6, 1e-4, or 0.1 per virus, (C) increasing the rate of infected cell death (δ_1+) with Function (2.8) for κ = 1e-6, 1e-5 or 1 per virus, or (D) increasing the rate of viral clearance (c_1+) with Function (2.8) for κ =1e-6, 1e-4, or 1 per virus. The strength of interaction compared to viral loads for (E) Virus 1 or (F) Virus 2 for the given interactions. Parameters are given in Table 2.1.

2.3.2 Effect of Relative Timing of Infection on Viral Kinetics

There is a critical time window of infection in which the two viruses can interact, which for our parameters is -1 to 2 days post infection. If the viruses infect the host within this time window, then viral kinetics are qualitatively similar regardless of timing (Figure 2.6) and (Figure 2.7). Scenarios in which Virus 2 infects 1 day prior to Virus 1 led to similar viral kinetics as simultaneous infections (Figures 2.2–2.3) and (Figures 2.6–2.7).

We further compared the relative timing of infections by varying the infection start times for both viruses, Virus 1 and Virus 2. While the viral kinetics are qualitatively similar with variable timing of infections as simultaneous coinfection, the total virus produced strongly depends on the relative timing of viruses (Figure 2.8). When Virus 1 is enhanced by the presence of Virus 2, the largest effect occurs if the host is infected with Virus 1 between one and two days after Virus 2 (Figure 2.8A). When Virus 1 is inhibited by the presence of Virus 2, the viral curves produce similar dynamics, the fold change in Virus 1 is one and then decays to minus one, but the time it takes to reach minus one varies for decreasing the infection rate (β_1-), decreasing the viral production rate (p_1-), increasing the viral clearance rate (c_1+), and increasing the infected cell death rate (δ_1+). (Figure 2.8B). The fold change in Virus 2 ranges between minus one and one for both enhancement and inhibition of Virus 1 (Figure 2.8A–B).

The strength of interaction plays a role in determining the magnitude and timing of the viral peaks (Figures 2.8–2.9). For large κ values (κ=1e-4), rates that enhance Virus 1 can lead to large amounts of virus compared to the baseline (Figure 2.8A). As the strength of interaction between viruses is reduced, the fold change in Virus 1 is reduced for rates that enhance Virus 1 (Figure 2.9B).

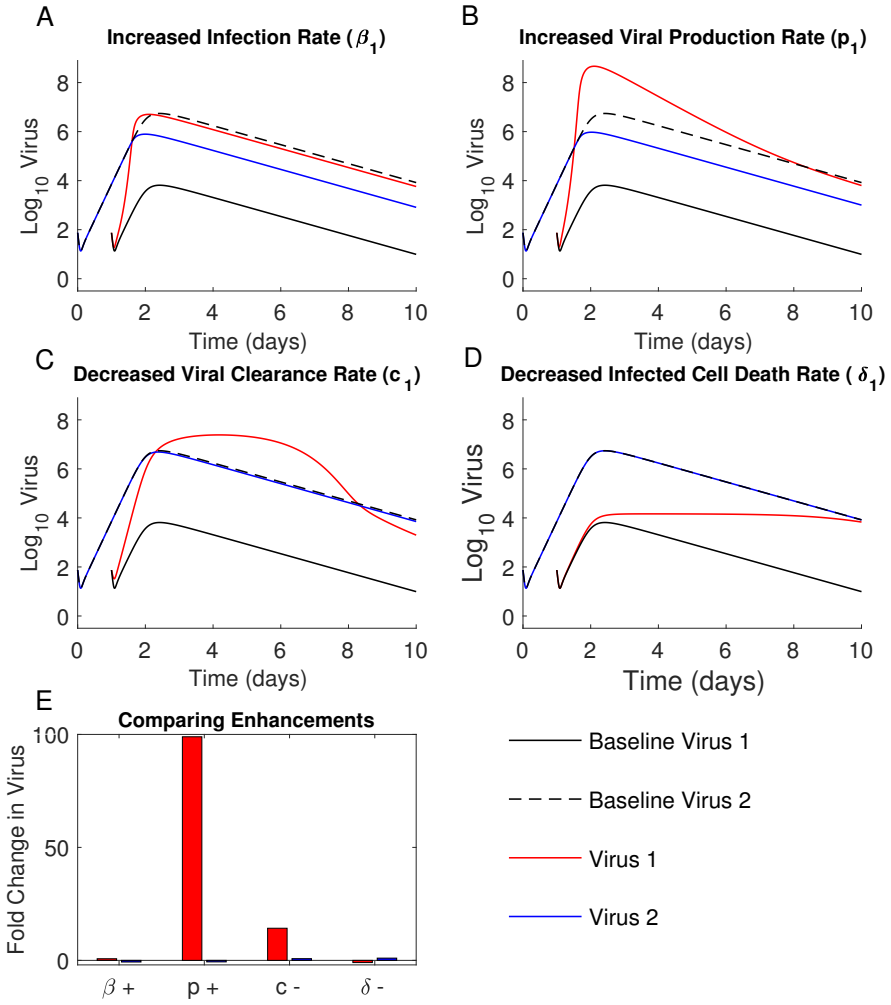

Figure 2.6: Effect of timing of infections on viral kinetics during positive virus interference. Equations (2.1)–(2.7) together with Equation (2.8) or Equation (2.9) were used to simulate the interaction of two viruses in cases where the interaction of Virus 2 on Virus 1 leads to an increase in viral titers with Virus 2 infecting one day before Virus 1. Panels A–D show comparisons of Virus 1 and 2 for the model without interaction, Virus 1 baseline (black dotted lines), and Virus 2 baseline (black solid lines), against the given interaction, Virus 1 (red), and Virus 2 (blue). (A) shows an increase in the infection rate (β_1), (B) shows an increase in the production rate (p_1), (C) shows a decrease in viral clearance rate, c_1 and (D) shows a decrease in infected cell death rate (δ_1). (E) shows the fold change in virus titers compared to the baseline titers for Virus 1 (red bars), or Virus 2 (blue bars). Parameters were taken from Table 2.1 with the strength of interaction, $\kappa = 10^{-4}$ per virus, all other parameters are given in Table 2.1.

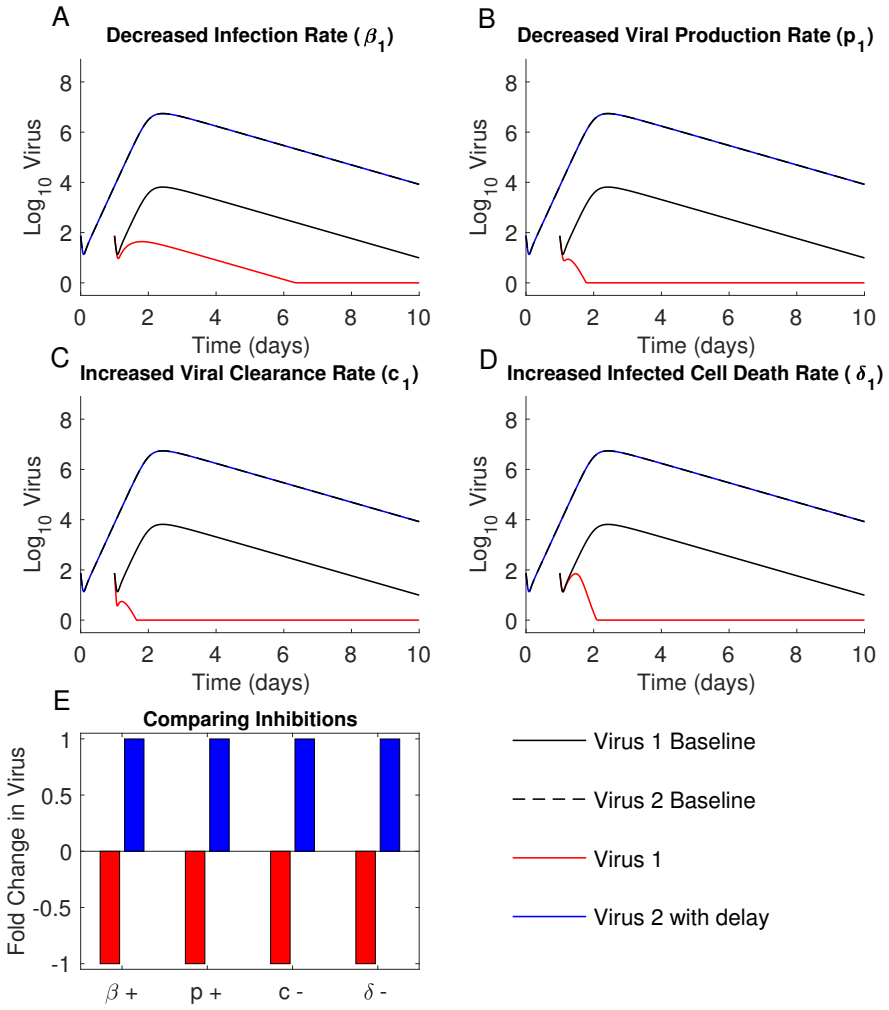

Figure 2.7: Effect of timing of infections on viral kinetics during negative virus interference. Equations (2.1)–(2.7) together with Equation (2.8) or Equation (2.9) were used to simulate the interaction of two viruses in cases where the interaction of Virus 2 on Virus 1 leads to an decrease in viral titers with Virus 2 infecting one day before Virus 1. Panels A–D show comparisons of Virus 1 and 2 for the model without interaction, Virus 1 baseline (black dotted lines), and Virus 2 baseline (black solid lines), against the given interaction, Virus 1 (red), and Virus 2 (blue). (A) shows a decrease in the infection rate (β_1), (B) shows a decrease in the production rate (p_1), (C) shows an increase in viral clearance rate, c_1 and (D) shows an increase in infected cell death rate (δ_1). (E) shows the fold change in virus titers compared to the baseline titers for Virus 1 (red bars), or Virus 2 (blue bars). Parameters were taken from Table 2.1 with the strength of interaction, $\kappa = 10^{-4}$ per virus, all other parameters are given in Table 2.1.

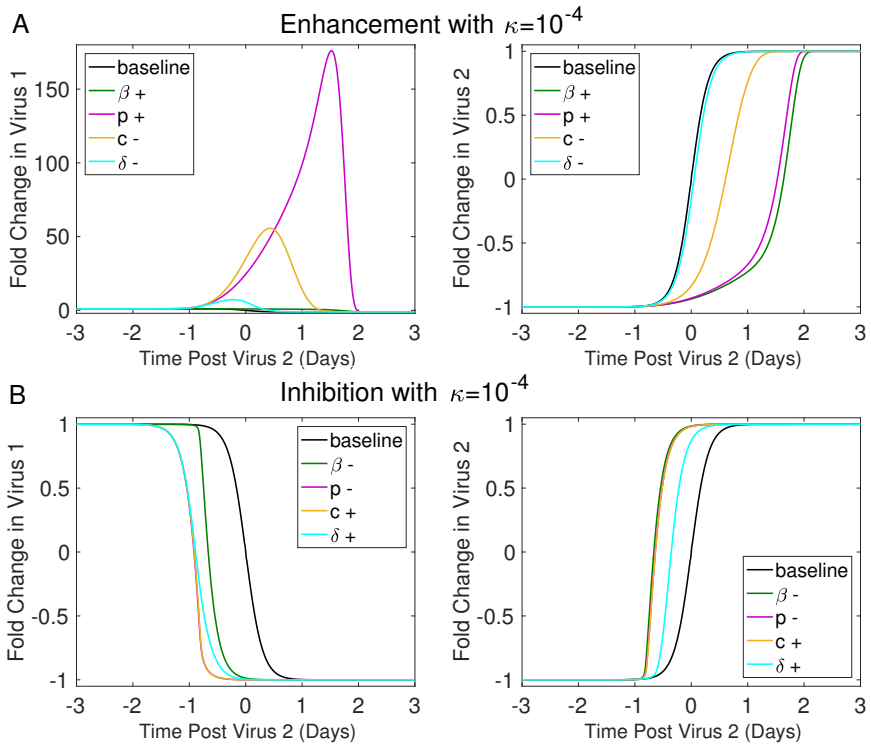

Figure 2.8: Effect of timing of infections on total virus produced with strong interactions. Each panel shows the fold change in virus produced over the course of infection as a function of the relative timing of virus infections. Equations (2.1)–(2.7) together with Equation (2.8) or Equation (2.9) were numerically solved for a range of relative timings of infection between the two viruses. (A) shows the change in Virus 1 and Virus 2 for an increase in infection rate (β_1+) (green), an increase in virus production, (p_1+) (pink), a decrease in viral clearance, (c_1-) (yellow), and a decrease in infected cell death, (δ_1-) (cyan). (B) shows the change in Virus 1 and Virus 2 for a decrease in infection rate, (β_1-) (green), a decrease in virus production (p_1-) (pink), an increase in viral clearance (c_1+) (yellow), and an increase in infected cell death (δ_1+) (cyan). Parameters were given in Table 2.1 with κ=1e-4 per virus. Initial conditions were taken from the single infection model from [51] for the given infection start time.

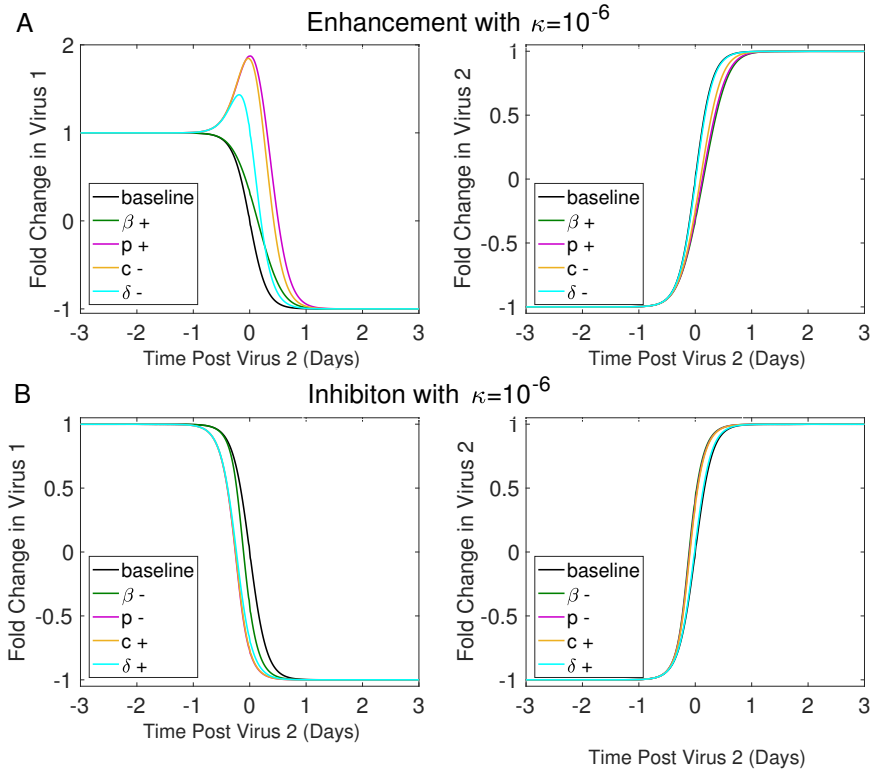

Figure 2.9: Effect of timing of infections on total virus produced with weak interactions. Each panel shows the fold change in virus produced over the course of infection as a function of the relative timing of virus infections. Equations (2.1)–(2.7) together with Equation (2.8) or Equation (2.9) were numerically solved for a range of relative timings of infection between the two viruses. (A) shows the change in Virus 1 and Virus 2 for an increase in infection rate (β_1+) (green), an increase in virus production, (p_1+) (pink), a decrease in viral clearance, (c_1-) (yellow), and a decrease in infected cell death, (δ_1-) (cyan). (B) shows the change in Virus 1 and Virus 2 for a decrease in infection rate, (β_1-) (green), a decrease in virus production (p_1-) (pink), an increase in viral clearance (c_1+) (yellow), and an increase in infected cell death (δ_1+) (cyan). Parameters were given in Table 2.1 with κ=1e-6 per virus. Initial conditions were taken from the single infection model from [51] for the given infection start time.

2.4 Discussion

Studies have shown patients can be infected by more than one virus [3, 4, 6, 9, 13, 53–57, 60]. In coinfection, interactions between multiple viruses within a host can increase disease severity and may enhance transmission while other interactions can reduce disease severity and possibly block the infection of a second virus [6, 11, 54, 55, 58]. Understanding the mechanisms that drive disease severity is important to prevent and treat viral infections. Experimental data on viral-viral coinfections is limited, but studies have shown that certain virus combinations increase viral loads while others decrease viral loads [10, 11, 58]. These interactions can be caused by numerous mechanisms that alter key rates that govern viral kinetics. While these mechanisms have not all yet been observed in respiratory viral coinfections, some mechanisms observed in other viral coinfections are blocking entry to cells decreasing infection rates, altering receptor expression increasing infection rates, modification of the interferon-induced antiviral state increasing or decreasing viral clearance or infected cell death rates, and viral exclusion decreasing infection or virus production rates [59, 60, 62].

Several studies have shown that viral-viral coinfections in the respiratory tract can have consequences *in vitro* and *in vivo* [10, 11, 56]. In one study, an *in vitro* cell culture system was used to investigate coinfection between PIV-2 and IAV [10]. In those experiments, IAV titers were elevated during PIV-IAV coinfection compared to a single infection while PIV titers were not altered. The authors further determined that PIV enhanced the fusion of epithelial cells to each other, and thus increased the growth rate of IAV [10]. In our model, numerous mechanisms are consistent with the increase in IAV titers during the growth phase, including increasing the infection rate ($\beta+$), increasing the viral production rate ($p+$), and decreasing the viral clearance rate ($c-$) (Figure 2.4). More data leading to higher resolution and longer time series in conjunction with our

mathematical model may allow us distinguish between these mechanisms.

There is a critical time window during which viruses can interact in coinfection. When IAV and RSV are coinfected within a ferret, IAV can reduce disease severity of RSV depending on the timing of infection of the two viruses. When RSV is introduced in the ferret 3 days or 7 days after IAV, disease severity of RSV is reduced by increasing the levels of pro-inflammatory cytokines within the respiratory tract; however, this effect is not observed when RSV is introduced 11 days after IAV. Moreover, when RSV was given before IAV, morbidity in the ferrets was reduced, but viral loads were similar [58]. These results are consistent with our model that timing of virus infections can affect viral dynamics and outcome (Figures 2.8–2.9).

Gonzalez et al. [11] also found that outcomes can depend on timing of infections and the virus pairing. In one set of experiments, when mice were infected with RV then IAV two days later, IAV titers were lower late in the infection. This corresponded with reduced inflammation. This effect was not seen *in vitro*, suggesting the interaction between the two viruses is not direct and may be mediated by the host response. They also found that when mice were infected with MHV two days before PR8, PR8 titers were reduced in lungs early in infection. This corresponded with an upregulation of IFN-β. Our model shows similar results when Virus 2 inhibits Virus 1 by increasing the infected cell death rate ($c+$) or viral clearance rate ($\delta+$), both of which could be mediated by immune responses (Figure 2.5C–D).

Some viruses are more likely to be detected in coinfection than others [3, 4, 6, 9, 13, 53–57]. Martin et al. [54] showed that ADV was the most commonly detected pathogen in multi-virus infection. Coronaviruses were also common, but disease severity was decreased in most multi-virus coinfections involving CoV [54]. Presently, the mechanisms underlying the increased frequency of ADV or CoV in coinfections is unknown. Our model may be useful for understanding why some viruses appear more often than others.

If a virus tends to benefit from coinfection, it may be more likely to be found in coinfected individuals than a virus that does not benefit from coinfection.

Our model focuses on the interaction between different respiratory viruses. We kept the virus inoculum (V_0) constant and focused on modifying a single rate at a time. However, Pinky and Dobrovolny [52] showed that varying the virus inoculum and infection rates could drastically change viral dynamics and the outcome of the coinfection. Pinky and Dobrovolny [52] used viral interference in the form of competition for target cells to explain the variation between viruses in coinfection. They also determined that a primary factor determining which virus outcompeted the other was the growth rate, which is a combination of the target cell infection rate (β) and viral production rate (p) [64]. Our model shows that modifying a single process either through enhancing the rate or inhibiting it, can also result in differences in viral titers, without needing to alter the virus inoculum (V_0) or changing the infection rates (β) of viruses.

By developing and analyzing a general mathematical model of within-host viral coinfection, we have mapped the landscape of how viral interactions affect viral kinetics and thus disease severity. While we considered respiratory viruses in parameterization, the model is general enough that it applies broadly to acute coinfections where both viruses target the same cells. As more temporal viral titer data become available in coinfection, comparisons with our model can serve to better interpret the data by generating hypotheses of underlying mechanisms governing viral interactions. With this information in hand, further studies can then be designed to test and verify mechanisms, ultimately leading to a more complete understanding of coinfection.

Bibliography

[1] Christopher Troeger, Mohammad Forouzanfar, Puja C. Rao, Ibrahim Khalil, Alexandria Brown, Scott Swartz, Nancy Fullman, Jonathan Mosser, Robert L Thompson, Robert C Reiner Jr, et al. Estimates of the global, regional, and national morbidity, mortality, and aetiologies of lower respiratory tract infections in 195 countries: a systematic analysis for the Global Burden of Disease Study 2015. *The Lancet Infectious Diseases*, 17(11):1133–1161, 2017.

[2] William W. Thompson, David K. Shay, Eric Weintraub, Lynnette Brammer, Nancy Cox, Larry J. Anderson, and Keiji Fukuda. Mortality associated with influenza and respiratory syncytial virus in the united states. *The Journal of the American Medical Association*, 289(2):179–186, 2003.

[3] Seema Jain, Derek J. Williams, Sandra R. Arnold, Krow Ampofo, Anna M. Bramley, Carrie Reed, Chris Stockmann, Evan J Anderson, Carlos G. Grijalva, Wesley H. Self, et al. Community-acquired pneumonia requiring hospitalization among US children. *New England Journal of Medicine*, 372(9):835–845, 2015.

[4] Seema Jain, Wesley H. Self, Richard G. Wunderink, Sherene Fakhran, Robert Balk, Anna M. Bramley, Carrie Reed, Carlos G. Grijalva, Evan J. Anderson, D. Mark Courtney, et al. Community-acquired pneumonia requiring hospitalization among US adults. *New England Journal of Medicine*, 373(5):415–427, 2015.

[5] Hervé Pascalis, Sarah Temmam, Magali Turpin, Olivier Rollot, Antoine Flahault, Fabrice Carrat, Xavier De Lamballerie, Patrick Gérardin, and Koussay Dellagi. Intense co-circulation of non-influenza respiratory viruses during the first wave of pandemic influenza pH1N1/2009: A cohort study in Reunion Island. *PLoS One*, 7 (9):e44755, 2012.

[6] Ristan M. Greer, Peter McErlean, Katherine E. Arden, Cassandra E. Faux, Andreas Nitsche, Stephen B. Lambert, Michael D. Nissen, Theo P. Sloots, and Ian M. Mackay. Do rhinoviruses reduce the probability of viral co-detection during acute respiratory tract infections? *Journal of Clinical Virology*, 45(1):10–15, 2009.

[7] Gabriel Ånestad and Svein A. Nordbø. Virus interference. Did rhinoviruses activity hamper the progress of the 2009 influenza A (H1N1) pandemic in Norway? *Medical Hypotheses*, 77(6):1132–1134, 2011.

[8] Caroline B. Hall. Respiratory syncytial virus and parainfluenza virus. *New England Journal of Medicine*, 344(25):1917–1928, 2001.

[9] Edward A. Goka, Pamela J. Vallely, Kenneth J. Mutton, and Paul E. Klapper. Single and multiple respiratory virus infections and severity of respiratory disease: A systematic review. *Paediatric Respiratory Reviews*, 15(4):363 – 370, 2014. ISSN 1526-0542.

[10] Hideo Goto, Hironobu Ihira, Keiichi Morishita, Mitsuki Tsuchiya, Keisuke Ohta, Natsuko Yumine, Masato Tsurudome, and Machiko Nishio. Enhanced growth of influenza A virus by coinfection with human parainfluenza virus type 2. *Medical Microbiology and Immunology*, 205(3):209–218, 2016.

[11] Andres J. Gonzalez, Emmanuel C. Ijezie, Onesmo B. Balemba, and Tanya A. Miura. Attenuation of influenza A virus disease severity by viral coinfection in a mouse model. *Journal of Virology*, 92(23), 2018. ISSN 0022-538X.

[12] Jia Meng, Christopher C. Stobart, Anne L. Hotard, and Martin L. Moore. An overview of respiratory syncytial virus. *PLoS Pathogens*, 10(4):e1004016, 2014.

[13] Nicole M. Bouvier and Peter Palese. The biology of influenza viruses. *Vaccine*, 26: D49–D53, 2008.

[14] Ian A. Wilson, John J. Skehel, and Don C. Wiley. Structure of the haemagglutinin membrane glycoprotein of influenza virus at 3 å resolution. *Nature*, 289(5796):366, 1981.

[15] Robert G. Webster, William J. Bean, Owen T. Gorman, Thomas M. Chambers, and Yoshihiro Kawaoka. Evolution and ecology of influenza A viruses. *Microbiological Reviews*, 56(1):152–179, 1992.

[16] Jochen Gottschalk, Reinhard Zbinden, Lucia Kaempf, and Ivo Heinzer. Discrimination of respiratory syncytial virus subgroups A and B by reverse transcription-PCR. *Journal of Clinical Microbiology*, 34(1):41–43, 1996.

[17] Florian Krammer and Peter Palese. Advances in the development of influenza virus vaccines. *Nature Reviews Drug Discovery*, 14(3):167, 2015.

[18] Robert Cruickshank. *Medical microbiology: The practice of medical microbiology*, volume 2. Churchill Livingstone, 1975.

[19] Laura P. Newman, Niranjan Bhat, Jessica A. Fleming, and Kathleen M. Neuzil. Global influenza seasonality to inform country-level vaccine programs: An analysis of WHO FluNet influenza surveillance data between 2011 and 2016. *PLoS One*, 13 (2):e0193263, 2018.

[20] Arnold S. Monto. The seasonality of rhinovirus infections and its implications for clinical recognition. *Clinical Therapeutics*, 24(12):1987–1997, 2002.

[21] Gordon Abraham and Richard J. Colonno. Many rhinovirus serotypes share the same cellular receptor. *Journal of Virology*, 51(2):340–345, 1984.

[22] Alicia M. Fry, Aaron T. Curns, Kathryn Harbour, Lori Hutwagner, Robert C. Holman, and Larry J. Anderson. Seasonal trends of human parainfluenza viral

infections: United States, 1990–2004. *Clinical Infectious Diseases*, 43(8):1016–1022, 2006.

[23] Judith H. Aberle, Stephan W. Aberle, Monika Redlberger-Fritz, Michael J. Sandhofer, and Therese Popow-Kraupp. Human metapneumovirus subgroup changes and seasonality during epidemics. *The Pediatric Infectious Disease Journal*, 29 (11):1016–1018, 2010.

[24] Bernadette G. Van den Hoogen, Sander Herfst, Leo Sprong, Patricia A. Cane, Eduardo Forleo-Neto, Rik L. De Swart, Albert DME. Osterhaus, and Ron AM. Fouchier. Antigenic and genetic variability of human metapneumoviruses. *Emerging Infectious Diseases*, 10(4):658, 2004.

[25] Sallene Wong, Kanti Pabbaraju, Xiaoli L. Pang, Bonita E. Lee, and Julie D. Fox. Detection of a broad range of human adenoviruses in respiratory tract samples using a sensitive multiplex real-time PCR assay. *Journal of Medical Virology*, 80 (5):856–865, 2008.

[26] Hulda R. Jonsdottir and Ronald Dijkman. Coronaviruses and the human airway: A universal system for virus-host interaction studies. *Virology Journal*, 13(1):24, 2016.

[27] Eleanor R. Gaunt, Andrew Hardie, Eric C. J. Claas, Peter Simmonds, and Kate E. Templeton. Epidemiology and clinical presentations of the four human coronaviruses 229E, HKU1, NL63, and OC43 detected over 3 years using a novel multiplex real-time PCR method. *Journal of Clinical Microbiology*, 48(8):2940–2947, 2010.

[28] Amber M. Smith and Alan S. Perelson. Influenza A virus infection kinetics: quantitative data and models. *Wiley Interdisciplinary Reviews: Systems Biology and Medicine*, 3(4):429–445, 2011.

[29] Pieter Mestdagh, Pieter Van Vlierberghe, An De Weer, Daniel Muth, Frank Westermann, Frank Speleman, and Jo Vandesompele. A novel and universal method for microRNA RT-qPCR data normalization. *Genome biology*, 10(6):R64, 2009.

[30] Alan Baer and Kylene Kehn-Hall. Viral concentration determination through plaque assays: using traditional and novel overlay systems. *Journal of Visualized Experiments*, (93), 2014.

[31] Rob E. Ploemacher, Johannes P. van der Sluijs, JS. Voerman, and NH. Brons. An in vitro limiting-dilution assay of long-term repopulating hematopoietic stem cells in the mouse. *Blood*, 74(8):2755–2763, 1989.

[32] Alan S. Perelson. Modelling viral and immune system dynamics. *Nature Reviews Immunology*, 2(1):28, 2002.

[33] Martin A. Nowak and Robert M. May. *Virus dynamics: Mathematical principles of immunology and virology*. Oxford university press, 2000.

[34] Andreas Handel, Laura E. Liao, and Catherine AA. Beauchemin. Progress and trends in mathematical modelling of influenza A virus infections. *Current Opinion in Systems Biology*, 2018.

[35] Amber M. Smith. Host-pathogen kinetics during influenza infection and coinfection: Insights from predictive modeling. *Immunological Reviews*, 285(1):97–112, 2018.

[36] Amber M. Smith. Validated models of immune response to virus infection. *Current Opinion in Systems Biology*, 2018.

[37] Stanca M. Ciupe and Jane M. Heffernan. In-host modeling. *Infectious Disease Modelling*, 2(2):188–202, 2017.

[38] Anushree Chatterjee, Jeremie Guedj, and Alan S. Perelson. Mathematical modeling of HCV infection: What can it teach us in the era of direct antiviral agents? *Antiviral Therapy*, 17(6 0 0):1171, 2012.

[39] Alan S. Perelson, Avidan U. Neumann, Martin Markowitz, John M. Leonard, David D. Ho, et al. HIV-1 dynamics in vivo: virion clearance rate, infected cell life-span, and viral generation time. *Science*, 271(5255):1582–1586, 1996.

[40] Martin A. Nowak, Sebastian Bonhoeffer, Andrew M. Hill, Richard Boehme, Howard C. Thomas, and Hugh McDade. Viral dynamics in hepatitis B virus infection. *Proceedings of the National Academy of Sciences*, 93(9):4398–4402, 1996.

[41] Stanca M. Ciupe, Ruy M. Ribeiro, Patrick W. Nelson, Geoffrey Dusheiko, and Alan S. Perelson. The role of cells refractory to productive infection in acute hepatitis B viral dynamics. *Proceedings of the National Academy of Sciences*, 104(12): 5050–5055, 2007.

[42] Harel Dahari, Jennifer E. Layden-Almer, Eric Kallwitz, Ruy M. Ribeiro, Scott J. Cotler, Thomas J. Layden, and Alan S. Perelson. A mathematical model of hepatitis C virus dynamics in patients with high baseline viral loads or advanced liver disease. *Gastroenterology*, 136(4):1402–1409, 2009.

[43] Soumya Banerjee, Jeremie Guedj, Ruy M. Ribeiro, Melanie Moses, and Alan S. Perelson. Estimating biologically relevant parameters under uncertainty for experimental within-host murine West Nile virus infection. *Journal of the Royal Society Interface*, 13(117):20160130, 2016.

[44] Bianca Schmid, Melanie Rinas, Alessia Ruggieri, Eliana G. Acosta, Marie Bartenschlager, Antje Reuter, Wolfgang Fischl, Nathalie Harder, Jan-Philip Bergeest, Michael Flossdorf, et al. Live cell analysis and mathematical modeling identify

determinants of attenuation of dengue virus 2'$-O-$methylation mutant. *PLoS Pathogens*, 11(12):e1005345, 2015.

[45] Yan Li and Andreas Handel. Modeling inoculum dose dependent patterns of acute virus infections. *Journal of Theoretical Biology*, 347:63–73, 2014.

[46] James Moore, Hasan Ahmed, Jonathan Jia, Rama Akondy, Rafi Ahmed, and Rustom Antia. What controls the acute viral infection following yellow fever vaccination? *Bulletin of Mathematical Biology*, 80(1):46–63, 2018.

[47] Katharine Best, Jeremie Guedj, Vincent Madelain, Xavier de Lamballerie, So-Yon Lim, Christa E. Osuna, James B. Whitney, and Alan S. Perelson. Zika plasma viral dynamics in nonhuman primates provides insights into early infection and antiviral strategies. *Proceedings of the National Academy of Sciences*, 114(33):8847–8852, 2017.

[48] Arturo Blazquez-Navarro, Thomas Schachtner, Ulrik Stervbo, Anett Sefrin, Maik Stein, Timm H. Westhoff, Petra Reinke, Edda Klipp, Nina Babel, Avidan U. Neumann, et al. Differential T cell response against BK virus regulatory and structural antigens: A viral dynamics modelling approach. *PLoS Computational Biology*, 14 (5):e1005998, 2018.

[49] Carmen Lía Murall, Robert Jackson, Ingeborg Zehbe, Nathalie Boulle, Michel Segondy, and Samuel Alizon. Epithelial stratification shapes infection dynamics. *bioRxiv*, page 231985, 2017.

[50] Meghna Verma, Samantha Erwin, Vida Abedi, Raquel Hontecillas, Stefan Hoops, Andrew Leber, Josep Bassaganya-Riera, and Stanca M. Ciupe. Modeling the mechanisms by which HIV-associated immunosuppression influences HPV persistence at the oral mucosa. *PLoS One*, 12(1):e0168133, 2017.

[51] Prasith Baccam, Catherine Beauchemin, Catherine A. Macken, Frederick G. Hayden, and Alan S. Perelson. Kinetics of influenza A virus infection in humans. *Journal of Virology*, 80(15):7590–7599, 2006.

[52] Lubna Pinky and Hana M. Dobrovolny. Coinfections of the respiratory tract: viral competition for resources. *PLoS One*, 11(5):e0155589, 2016.

[53] David M. Morens, Jeffery K. Taubenberger, and Anthony S. Fauci. Predominant role of bacterial pneumonia as a cause of death in pandemic influenza: Implications for pandemic influenza preparedness. *Journal of Infectious Diseases*, 198(7), 2008.

[54] Emily T. Martin, Jane Kuypers, Anna Wald, and Janet A. Englund. Multiple versus single virus respiratory infections: viral load and clinical disease severity in hospitalized children. *Influenza and Other Respiratory Viruses*, 6(1):71–77, 2012.

[55] Judith H. Aberle, Stephan W. Aberle, Elisabeth Pracher, Hans-Peter Hutter, Michael Kundi, and Therese Popow-Kraupp. Single versus dual respiratory virus infections in hospitalized infants: Impact on clinical course of disease and interferon-γ response. *The Pediatric Infectious Disease Journal*, 24(7):605–610, 2005.

[56] Ilona Stefanska, Malgorzata Romanowska, Stefan Donevski, Dariusz Gawryluk, and Lidia B. Brydak. Co-infections with influenza and other respiratory viruses. In *Respiratory Regulation-The Molecular Approach*, pages 291–301. Springer, 2013.

[57] Marcelo C. Scotta, Valentina C. B. Gava Chakr, Angela de Moura, Rafaela Garces Becker, Ana Paula Duarte de Souza, Marcus Herbert Jones, Leonardo Araújo Pinto, Edgar Enrique Sarria, Paulo Marcio Pitrez, Renato Tetelbom Stein, et al. Respiratory viral coinfection and disease severity in children: A systematic review and meta-analysis. *Journal of Clinical Virology*, 80:45–56, 2016.

[58] Kok F. Chan, Louise A. Carolan, Daniil Korenkov, Julian Druce, James McCaw, Patrick C. Reading, Ian G. Barr, and Karen L. Laurie. Investigating viral interference between influenza A virus and human respiratory syncytial virus in a ferret model of infection. *The Journal of Infectious Diseases*, 2018.

[59] Werner Henle. Interference phenomena between animal viruses: A review. *The Journal of Immunology*, 64(3):203–236, 1950.

[60] Marshall G. Findlay and Frederick O. MacCallum. An interference phenomenon in relation to yellow fever and other viruses. *The Journal of Pathology and Bacteriology*, 44(2):405–424, 1937.

[61] Christoper H. Andrewes. Interference by one virus with the growth of another in tissue-culture. *British Journal of Experimental Pathology*, 23(4):214, 1942.

[62] Telma DaPalma, Bently P. Doonan, Nicole M. Trager, and Laura M. Kasman. A systematic approach to virus–virus interactions. *Virus Research*, 149(1):1–9, 2010.

[63] Amber M. Smith, Frederick R. Adler, Ruy M. Ribeiro, Ryan N. Gutenkunst, Julie L. McAuley, Jonathan A. McCullers, and Alan S. Perelson. Kinetics of coinfection with influenza A virus and Streptococcus pneumoniae. *PLoS Pathogens*, 9(3):e1003238, 2013.

[64] Amber M. Smith, Frederick R. Adler, and Alan S. Perelson. An accurate two-phase approximate solution to an acute viral infection model. *Journal of Mathematical Biology*, 60(5):711–726, 2010.